



Numerical Modelling of Transport Phenomena and Macrosegregation during Ternary Alloy Solidification: Solutal Undercooling Effects

S. Ganguly[†]

R &D, Tata Steel Ltd., Jamshedpur, Jharkhand, 831007, India

[†]Corresponding Author Email: suva_112@yahoo.co.in

(Received April 17, 2018; accepted September 2, 2018)

ABSTRACT

In this paper, a macroscopic mathematical model is developed for simulation of transport phenomena during ternary alloy solidification processes, taking into account non-equilibrium effects due to solutal undercooling. The model is based on a fixed-grid, enthalpy-based, control volume approach. Microscopic features pertaining to non-equilibrium effects on account of solutal undercooling are incorporated through a novel formulation of a modified partition coefficient. The effective partition coefficient is numerically modeled by means of macroscopic parameters related to the solidifying domain. Numerical simulations are performed for ternary steel alloy by employing the present model and the resulting convection and macrosegregation patterns are analyzed. It is observed that the consideration of non-equilibrium solidification in the present mathematical approach is able to capture the thermo-solutal convection and leads to prediction of accurate value of macrosegregation. The results from the present model matches well with the experimental observations published in the literature.

Keywords: Solidification; Modelling; Convection; Macrosegregation.

NOMENCLATURE

Nomenclature should be in alphabetic order (A – Z) and Greek letters should follow after Latin letters in alphabetic order (α, β, \dots).

C	species concentration	K	permeability
c	specific heat	L	latent heat
D	diffusion coefficient	T	temperature
f	mass fraction	u	velocity component in x-direction
g	volume fraction	v	velocity component in y-direction
h	specific enthalpy		
h_c	convective heat transfer coefficient	μ	dynamic viscosity
ΔH	latent enthalpy	ρ	density

1. INTRODUCTION

Research efforts towards accurate mathematical modelling of alloy solidification process have been reported in the past (Prescott and Incropera 1996; Choudhary and Mazumdar 1994; Kang *et al.* 2005; Ganaoui *et al.* 2002; Ganguly *et al.* 2013). The role of macroscopic transport phenomena during solidification has been discussed in detail by many researchers (Brent *et al.* 1988; Ganesan and Poirier 1990). The freezing of a solid involves many complex physical issues which determine the transport behavior governing the phase-transition process during solidification. The interactions of the

solidifying melt with the two-phase mushy region in the presence of both temperature gradient and solute concentration gradient produces a resultant flow known as double-diffusive convection. This thermo-solutal convection drives the rejected solute elements away from the solid-liquid interface leading to a composition variation in the domain, thereby giving rise to macrosegregation (Flemings 1974).

Several studies have been undertaken to characterize the fluid flow and the development of macrosegregation during solidification. Initial studies started with moving-grid multiple-domain formulations (Gadgil and Gobin 1984), followed by

single-domain continuum formulation (Bennon and Incropera 1987; Voller *et al.* 1989). These studies have highlighted the important role of thermo-solutal convection in the long-range transport of solute and final macrosegregation pattern. An important aspect in this context is proper accounting of microscopic issues in the macroscopic model that dictate the macrosegregation behavior of the cast product. Prediction of local solute redistribution is generally given by Scheils equation (Flemings 1974) and is widely accepted. The model proposed by Brody and Flemings (1966) takes into consideration the diffusion in the solid phase and provides an improvement of the Scheils model. Clyne and Kurz (1981) presented a model for solute redistribution with rapid solid state diffusion. Kobayashi (1988) presented a modified macrosegregation model under the conditions of constant diffusion coefficient of solute in the solid, constant equilibrium partition-ratio, and parabolic growth. It can be noted here that during solidification, due to finite diffusivity in the liquid phase, there may be accumulation of solute within a diffusion boundary layer adjacent to the interface. This gives rise to a concentration gradient at the interface, which in turn, causes a local change in the liquidus temperature. This is commonly known as solutal undercooling, and is primarily governed by liquid species diffusivity, dendrite growth rate, thickness of the solutal boundary layer and the interface geometry (Rappaz 1989; Chakraborty *et al.* 2002). In all the previous studies, solutal undercooling effect is essentially neglected while modelling solidification. However, for accurate prediction of the final macrosegregation pattern in the solidified product, it is imperative that macroscopic model for multicomponent systems should represent pertinent microscopic issues within the macroscopic framework in a metallurgically consistent manner. Although there are attempts to incorporate the effect of solutal undercooling through ‘micro-macro modelling’ (Rappaz 1989), similar considerations in the framework of macroscopic modelling of multicomponent solidification is very rare. Also, model for ternary alloy systems, which can characterize relevant microscopic issues in the macroscopic framework in the presence of convective flow field, is not yet available in the literature. Towards this, the present research endeavour is a novel attempt to capture the intricate characteristics of non-equilibrium solidification, flow and macrosegregation.

In the present work, a macroscopic mathematical model for ternary alloy solidification is developed, with particular emphasis on non-equilibrium solidification considerations. The numerical approach is essentially based on fixed-grid enthalpy-based continuum formulation (Bennon and Incropera 1987; Voller *et al.* 1989). Microscopic features arising out of non-equilibrium effects due to solutal undercooling are incorporated through a novel formulation of modified partition-coefficient. The numerical implementation of the proposed algorithm correlates the microscopic features with the overall convection field, thereby presenting a method for accurate prediction of final

macrosegregation behavior.

2. MATHEMATICAL MODELLING

The following section outlines the mathematical modelling procedure and the solution techniques.

2.1 Governing Equations

A two-dimensional rectangular mould containing liquid ternary metal alloy is considered, where the boundary walls are subjected to different heat transfer conditions as depicted in Fig. 1. Unidirectional solidification takes place from the left boundary with the initial and boundary conditions shown in Fig. 1.

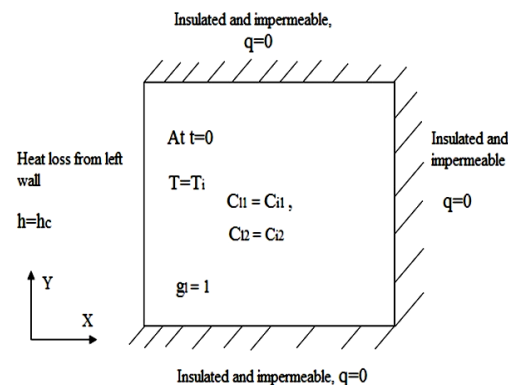


Fig. 1. Computational domain with boundary specifications.

Following a fixed-grid continuum formulation with a single-domain approach (Bennon and Incropera 1987), the governing equations for mass, momentum, energy and species transport can be written as follows

$$\frac{\partial \rho}{\partial t} + \nabla \cdot (\rho \vec{u}) = 0 \quad (1)$$

$$\frac{\partial (\rho \vec{u})}{\partial t} + \rho \vec{u} \cdot (\nabla \vec{u}) = \nabla \cdot \left(\mu_l \nabla \frac{\rho}{\rho_l} \vec{u} \right) - \nabla p + \vec{S}_u + S_b \quad (2)$$

Equations (1) and (2) are continuity equation and momentum equation respectively.

Here ρ, \vec{u}, μ, p , are the density, velocity, viscosity, and pressure respectively, and the subscript ‘*l*’ denotes the liquid phase. In Eq. (2), S_u denotes source term representing the flow resistance in the multiphase region and is a function of the morphology of the solid-liquid mushy region. These source terms are evaluated from Darcy’s model (Morvan *et al.* 1999) of viscous flow through a porous medium (assuming zero velocity of solid phase and isotropic permeability) as,

$$S_i = \frac{\mu_l \rho u_i}{K \rho_l} \quad (3)$$

where S_i denotes the source term corresponding to

velocity u_i in the appropriate direction and K is permeability. For the purpose of modeling the above term, K is prescribed as a function of liquid volume fraction (g_l). Towards this, the Carman-Kozeny relation (Brent *et al.* 1988) is used within a range of validity of $0 < g_l < 0.5$, i.e.,

$$K = K_0 \frac{g_l^3}{(1-g_l)^2} \quad (4)$$

Here, K_0 is porosity constant. It may be mentioned here that the above-mentioned Carman-Kozeny relation is found to be reasonably valid till the liquid fraction (g_l) attains a value of 0.5, which is the critical value of liquid fraction (g_l^{cr}) for application of the Carman-Kozeny model. For $g_l > 0.5$, a hybrid model is used (Morvan *et al.* 1999),

$$\mu_l = \mu_l^o \left(\frac{A_\mu}{A_\mu - Fg_s} \right)^2 \quad (5)$$

$$K = GK_0 \frac{g_l^3}{(1-g_l)^2} \quad \text{where } A_\mu = 0.4 \quad (6)$$

Here, F and G are described according to the rheology of suspensions (Brenner 1970) as,

$$F = 0.5 - \frac{1}{\pi} \arctan[100(g_l^{cr} - g_l)] \quad (7)$$

$$G = 0.5 + \frac{1}{\pi} \arctan[100(g_l^{cr} - g_l)]^4 \quad (8)$$

where $g_l^{cr} = 0.5$

Here, g_l^{cr} is the critical liquid fraction for application of Carman-Kozeny equation. It is worthwhile to mention here that in accordance with the physics of dendritic morphology occurring due to the evolution of solid dendrites in liquid matrix during phase change phenomena in multicomponent solidifying system (Morvan *et al.* 1999) several models are used in contemporary literature for accurate prediction of mushy zone flow physics (Oldenburg *et al.* 1992) and associated rheological characteristics (Brenner 1970). The rheology of suspensions (Brenner 1970) of solid in a liquid is a complex function of its physical properties and of processes that occur on the scale of the suspended solid particle morphology. Some important factors are volume fraction of different constituent phases, phase/particle interaction, nature of bulk flow field. In the present study, depending on the volume fraction of the liquid in the phase-changing domain, different functional forms describing the physics of solid-liquid interaction are identified for appropriate modelling of mushy zone fluid flow. Accordingly, depending on the local liquid volume fraction, permeability factor is determined and Eqs. (3) - (7) is used to evaluate the solid-liquid interaction force.

The buoyancy source term, S_b , in Eq. (2),

constitutes of both thermal and solutal effects, and is given by the differences between local and initial values of temperature and liquid solute concentrations, respectively. In the present context, density and concentrations are implicitly related through Boussinesq approximation, following the conventional assumption that the important density changes are those associated with buoyancy force in the liquid (solutal buoyancy and thermal buoyancy) (Ganaoui *et al.* 2002; Prescott and Incropera 1996). In the case of a ternary alloy, the buoyancy term in Eq. (2) can be written as:

$$S_b = \rho g [\beta_T (T - T_0) + \beta_{s1} (C_{l1} - C_{01}) + \beta_{s2} (C_{l2} - C_{02})] \quad (9)$$

Here, β_T and β_s are the thermal volumetric coefficient of expansion and solutal volumetric coefficient of expansion respectively, T_0 is the initial temperature, and C_0 is the initial solute concentration. Subscript '1' and '2' refer to element 1 and element 2 respectively.

The thermal energy conservation equation is given as follows:

$$\frac{\partial}{\partial t} (\rho T) + \nabla \cdot (\rho \bar{u} T) = \nabla \cdot \{ (g\Gamma + g\Gamma) \nabla T \} - \frac{1}{c} \left[\frac{\partial}{\partial t} (\rho g \Delta H) + \nabla \cdot (\rho \bar{u} \Delta H) \right] \quad (10)$$

where, $\Gamma_k = k_{Tk}/c_k$, and ΔH is the latent enthalpy.

here, g denotes volume fraction, and subscripts l and s corresponds to liquid and solid phases respectively. T is the temperature, c is the specific heat, and k is the thermal conductivity.

The species conservation equation is given as follows:

$$\frac{\partial}{\partial t} (\rho C_i) + \nabla \cdot (\rho \bar{u} C_i) = \nabla \cdot (D \nabla C_i) + S_c \quad (11)$$

Here, D is the mass diffusion coefficient and S_c is the source term. Equation (11) represents the general form of species conservation equation and is determined by the microstructure under consideration. In case of non-equilibrium solidification represented by a columnar dendritic microstructure, we have

$$D = \rho (g_s D_s k_p + g_l D_l) \quad (12)$$

$$S_c = \frac{\partial}{\partial t} (\rho g_s C_l) - k_p C_l \frac{\partial}{\partial t} (\rho g_s) \quad (13)$$

In the present case of a ternary alloy system, two independent species transport equations need to be considered; one equation for each constituent species. The relevant boundary conditions are as follows:

$$\text{Left wall: } u = 0, v = 0, -k \frac{\partial T}{\partial x} = h_c (T_\infty - T),$$

$$\partial(C_i)_1/\partial x=0, \partial(C_i)_2/\partial x=0 \quad (14)$$

$$\text{Right wall: } u = 0, v = 0, \frac{\partial T}{\partial x} = 0, \partial(C_i)_1/\partial x=0, \partial(C_i)_2/\partial x = 0 \quad (15)$$

$$\text{Top wall: } u = 0, v = 0, \frac{\partial T}{\partial y} = 0, \partial(C_i)_1/\partial y=0, \partial(C_i)_2/\partial y=0 \quad (16)$$

$$\text{Bottom wall: } u=0, v=0, \frac{\partial T}{\partial y} = 0, \partial(C_i)_1/\partial y=0, \partial(C_i)_2/\partial y=0 \quad (17)$$

Here, u and v are velocity components along x -axis and y -axis respectively, h_c is the convective heat transfer coefficient. The initial conditions are written as:

$$\text{At } t=0, u=0, T=T_i, (C_i)_1 = (C_i)_1, (C_i)_2 = (C_i)_2 \quad (18)$$

2.2 Modelling of Solutal Undercooling

For the purpose of modelling the microscopic advection effects, partition coefficient (k_p) in Eq. (13) has to be appropriately modified. The basis of such modification lies on the physics of macroscopic solidification models using the lever rule or Scheil's equation describing the microscopic solute conservation, with the assumption of well-mixed solute in the liquid state. In practice, the solute gets accumulated on the liquid phase within diffusion boundary layer next to the interface. This gives rise to 'solutal undercooling', which can be quantified as the difference between the interfacial and volume-averaged liquid species concentration. This primarily refers to a change in local liquidus temperature due to the change in species concentration and depend on the thermodynamic and physical properties, such as diffusivity, boundary layer thickness, morphological parameters, volume fraction etc. Solutal boundary layer characteristics at the interface affects the solute distribution in the bulk domain, which, again affects the convective flow field, resulting in overall macrosegregation pattern. Incorporation of such considerations in the macroscopic modeling framework calls for devising a method to capture the effect of solutal undercooling. Towards this, an effective partition coefficient (k_p^*) is defined and correlated with the equilibrium partition coefficient (k_p) as

$$k_p^* = \frac{k_p}{k_p + (1 - k_p)e^{(-R\delta/D_l)}} \quad (19)$$

Here k_p is given by the ratio of solid composition to bulk liquid composition, R is the rate of interface movement, δ is the diffusion boundary layer thickness, D_l is diffusion coefficient in the liquid phase. Equation (19) assumes immense significance as it relates the composition of solid to the alloy

composition and growth conditions. The parameter ($R\delta/D_l$) is often defined as the local solutal Peclet number and takes into account the effect of solutal undercooling. Above consideration is necessary to determine the overall flow behavior, and the final macro-segregation pattern.

3. NUMERICAL MODELLING

The coupled governing differential equations described in the preceding section are solved using a finite volume methodology (Patankar 1980). The transport equations are solved according to the SIMPLER algorithm (Patankar 1980). The above algorithm is appropriately modified to account for phase change considerations during non-equilibrium solidification due to solutal undercooling. This is achieved by modification of partition coefficient for convective effects in the algorithm. For the purpose of implementation, it is important to characterize the ratio of advection to diffusion strength defining the solutal Peclet number ($Pe = R\delta/D_l$). The convective strength can be expressed as $\chi \Delta V/\Delta A$, where χ is phase change rate per unit volume, ΔV is the volume of the control volume, ΔA is the solid-liquid interfacial area. The diffusion strength can be defined as $\rho D_L/l_{ref}$, where l_{ref} is the diffusion length scale in the liquid. The liquid-phase mass conservation equation is discretized to obtain the phase change rate as:

$$\frac{\partial(g_l \rho_l)}{\partial t} + \nabla \cdot (g_l \rho_l \bar{u}) = \chi \quad (20)$$

An implicit forward differencing scheme is adopted to discretize the transient term in Eq. (20). The convective source term is discretized using upwind formulation.

The strength of diffusive transport can be properly evaluated with prescription of macroscopic estimates of diffusion length scale made as,

$$\frac{D_L}{l_{ref}} = \frac{\bar{x}_t - \bar{x}_{t-\Delta t}}{\Delta t} \quad (21)$$

where \bar{x} is the location of the mushy-liquid interface and Δt is the time step.

For accurate prediction of the liquid fraction in the present enthalpy-based approach, the latent heat content of each computational cell is updated according to the temperature and/or species concentration values predicted by macroscopic conservation equations, during each iteration within a time step. In the present context, an iterative update scheme (Brent *et al.* 1988), is adopted as,

$$[\Delta H_p]_{n+1} = [\Delta H_p]_n + \frac{a_p}{a_p^0} \lambda [\{h_p\}_n - c_p F^{-1} \{\Delta H_p\}_n] \quad (22)$$

where ΔH_p is the latent heat content of the

Table 1 Thermodynamic parameters of elements for ternary alloy

Element	Carbon (C)	Manganese (Mn)	Nickel (Ni)
Cin (Wt %)	0.08	0.1	0.1
β_s (1/Wt %)	1.10×10^{-2}	1.92×10^{-3}	6.85×10^{-4}
DI (m2/s)	2.0×10^{-9}	2.0×10^{-9}	2.0×10^{-9}
Ds (m2/s)	5.6×10^{-10}	1.2×10^{-13}	1.9×10^{-13}
$\partial T_l / \partial C_l$ (K/Wt%)	-78	-3.32	-1.6
k_p	0.34	0.75	0.94

computational cell around grid point P , h is the sensible enthalpy, c_p is the specific heat, λ is a relaxation factor, n is the iteration level, a_p and a_p^0 are the coefficients of the finite volume discretization equation (Patankar 1980), and F^{-1} is the inverse of the latent heat function. It is to be noted here that in the above equation, F^{-1} needs to be devised consistently with the microscopic physics followed in the present mathematical formulation, so that accurate results pertaining to specific solidification model is obtained. For the non-equilibrium solidification situation with solutal undercooling, the function F^{-1} can be expressed as

$$F^{-1}(\Delta H) = c_p T_m - c_p (T_m - T_L) \left(\frac{\Delta H}{L} \right)^{k_p^* - 1} \quad (23)$$

where C_p is the specific heat of the mixture, L is the latent heat, T_m is the melting point of the solvent, T_L is the liquidus temperature, and k_p^* is the effective partition coefficient.

4. RESULTS & DISCUSSIONS

Numerical simulations are performed for the case of a (Fe-0.08wt%C-0.1wt%Mn) steel alloy with iron, carbon and manganese as the constituent elements. The liquidus temperature of the ternary steel alloy system for the present case is 1805 K, while the melt initially is at a uniform temperature of 1830K inside the domain. The heat transfer coefficient (h_c) at the left wall is taken as 125 W/m².K. Table 1 summarizes the species-dependent thermodynamic characteristics, as adopted in the present work. The relevant thermophysical properties for steel are listed in Table 2. Different grid sizes (40×40 , 60×60 and 100×100) are used for the resolution of the computational domain of size (0.1 m \times 0.1 m) to check for grid independence. For this purpose, magnitude of variation of solute concentration in the liquid is examined for optimum solution. It has been observed that the grid size of 60×60 produces computationally economical results with a variation of 0.25% among all the different cases studied in the present investigation. It is also found that further refinement in grid spacing does not alter the numerical predictions appreciably.

Table 2 Thermophysical properties of steel

Parameter	Value
Specific heat (c)	787 J/Kg. K
Thermal conductivity of solid (k_s)	30 W/m.K
Thermal conductivity of liquid (k_l)	27 W/m.K
Thermal expansion coefficient (β_T)	$2.0 \times 10^{-4} \text{ K}^{-1}$
Density (ρ)	7300 kg/m ³
Viscosity (μ)	$6.0 \times 10^{-4} \text{ kg/m.s}$
Latent heat of fusion (L)	$270 \times 10^3 \text{ J/kg}$

Figure 2 depicts the convection pattern for the selected alloy system, at time, $t=120$ s after beginning of solidification. Once cooling is started at the left vertical wall of the mould, the cold and dense fluid descends along the interface and turns near the bottom of the cavity, as demonstrated by the streamlines in Fig. 2. The streamlines show that the flow in the bulk melt is primarily counterclockwise, with a net downward flow occurring near the interface. With progress in solidification, rejected solute tends to reduce the mushy zone fluid density and guides the fluid in the upward direction. The streamlines also show the development of a minor vortex due to solutal buoyancy effects near the bottom corner of the cavity. The development of this minor vortex is due to solutal gradient build-up caused by the transportation of solute by the thermal buoyancy driven major vortex.

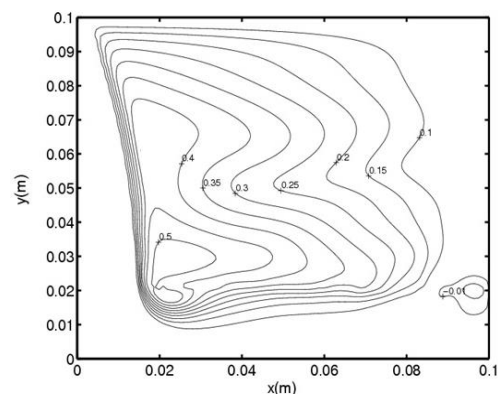


Fig. 2. Streamfunction plots at time =120 s for Fe-C-Mn steel alloy.

Figure 3 illustrates the composition variation of carbon along the longitudinal (x-axis) direction at different time intervals during the solidification of the present alloy system. For the purpose of comparison, present results are plotted along with those without the convection-correction of the partition-coefficient.

Figures 3(a)-3(b) shows the composition variation at t=100 s and t=200 s respectively, and at a vertical location y=0.05m. Rejection of solute during solidification leads to a sharp increase in solute concentration near the interface. The thermally driven flow, being dominant, carries the rejected solute downward along the interface giving rise to a composition variation. When the solutal undercooling effects are not considered, the global double-diffusive convection effects primarily controls the bulk fluid flow in the domain. However, with the consideration of solutal undercooling (present model), there is an additional influence of solutal convection due to solute build-up at the tip of the solidified dendrites. Owing to enhanced strength of resultant convective flow, the rejected solute species are transported more effectively resulting in composition variation in the domain. Neglecting such non-equilibrium effects due to undercooling may lead to the prediction of almost homogeneous composition distribution in the bulk domain with a flatter curve, as depicted in Fig. 3. Similar behavior is also observed for the composition variation of the other elements.

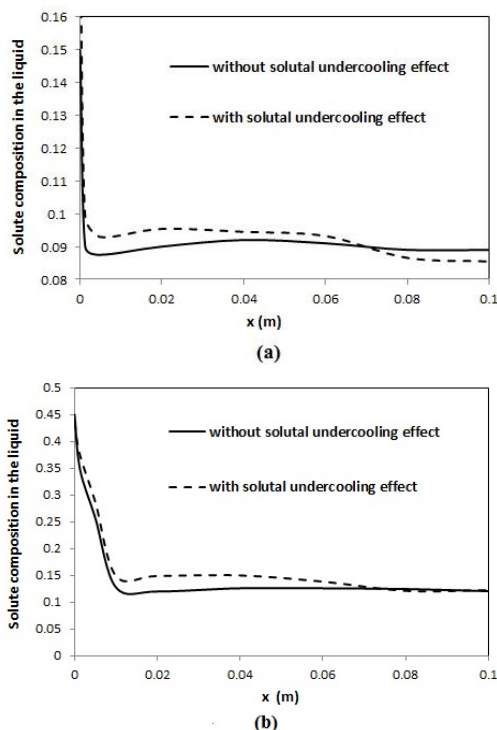


Fig. 3. Variation of liquid concentration in terms of mass fraction of solute (carbon) (a) at t = 100 sec (b) at t = 200 sec.

Figure 4 illustrates the development of macrosegregation of the constituent elements during

solidification. Macrosegregation effects are calculated as follows:

$$M(i) = \left[\frac{1}{V} \int_V \left(\frac{C_{mix,i}}{C_{o,i}} - 1 \right)^2 dV \right]^{1/2} \quad (24)$$

where the subscript ‘ i ’ denotes solute element under concern.

Figure 4(a) shows the macrosegregation of carbon and manganese for Fe-0.08wt% C-0.1wt%Mn alloy. In order to better quantify the novel simulation model developed in the present study, a separate case study is undertaken by changing the solute composition of the alloy system. Accordingly, Fig. 4(b) depicts the macrosegregation development for Fe-0.08wt% C-0.1wt%Ni alloy, for which the thermodynamic parameters are given in Table 1. Figures 4(a)-4(b) also compares the present model results with the case when no solutal undercooling effects are considered. For the particular case when the solutal undercooling effects are not incorporated in the model (i.e. no correction of k_p), the level of solute redistribution shows an initial rising trend, followed by asymptotic saturation of the concentration distribution. On the other hand, with the inclusion of non-equilibrium effects due to solutal undercooling, the additional strength of solutal convection intensifies the overall advective transport of the solute species in the flow domain, thereby giving rise to an enhanced value of macrosegregation. The solute concentration profile shows a rising trend for both the case studies as compared to the case when no solutal undercooling are considered. Overall, the macrosegregation distributions for the elements (carbon, manganese and nickel) are analogous with the segregation intensity depending on the partition coefficient of the element. In the alloy under consideration in the present study, the M_C value (i.e. carbon macrosegregation) is higher than M_{Mn} (i.e. macrosegregation for manganese) and M_{Ni} (i.e. macrosegregation for nickel), as seen from the Figs. 4(a)-4(b).

A comparative study between existing experimental data (Ferreira *et al.*2004) and present numerical simulation is performed. The reported experimental data in the literature refers to solidification of a ternary alloy system in a vertical water-cooled mold (Ferreira *et al.*2004). The casting assembly is a directionally solidified water-cooled mould and experiments were performed with Al8.1wt%-Cu3wt%-Si alloy, under controlled solidification conditions. The thermophysical properties of this alloy are given in Table 3.

Figure 5 compares the simulated macrosegregation level of copper and the corresponding experimental results (Ferreira *et al.*2004). It is observed that the predictions from the present model agrees well with

the corresponding experimental results; the average error being less than 0.5%, and the maximum difference is no more than 3.8% from the literature. It can be deduced from the preceding observation that the consideration of nonequilibrium phenomena arising out of solutal undercooling renders better predictive ability to the present model which lead to more accurate determination of the macrosegregation characteristics.

Table 3 Thermophysical properties of the Al-Cu-Si alloy

Parameter	Value
Specific heat (c)	1089 J/Kg. K
Thermal conductivity of solid (k_s)	191 W/m.K
Thermal conductivity of liquid (k_l)	88 W/m.K
Solute Diffusivity (D)	$3.5 \times 10^{-9} \text{ m}^2/\text{s}$
Density (ρ)	2698 kg/m ³
Partition coefficient (Cu/Si)	0.1015/0.1052
Liquidus slope (Cu/Si)	-3.39/-6.646 K/Wt%
Latent heat of fusion (L)	380 J/kg

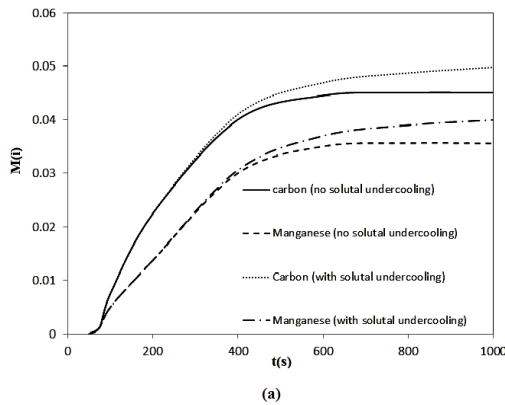


Fig. 4(a). Predicted carbon and manganese macrosegregation levels during solidification.

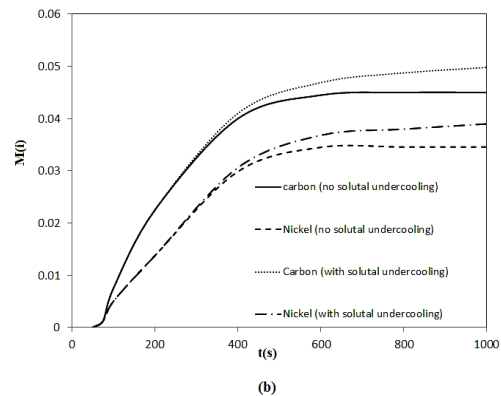


Fig. 4(b). Predicted carbon and nickel macrosegregation levels during solidification.

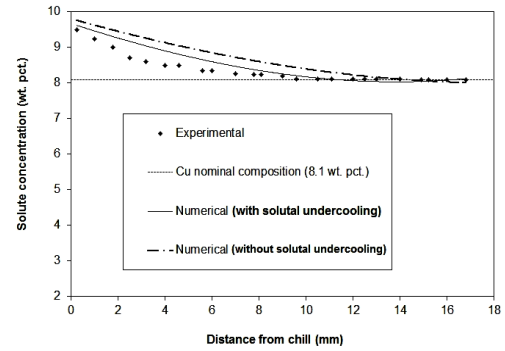


Fig. 5. Comparison between experimental results and numerical predictions.

5. CONCLUSION

In the present work, a macroscopic mathematical model is developed for studying transport phenomena and macrosegregation during ternary alloy solidification process. An attempt has been made to capture the non-equilibrium effects due to solutal undercooling by adopting a novel methodology based on fixed-grid, enthalpy-control volume approach. Numerical simulation for multicomponent steel alloy solidification is undertaken and the overall transport behaviour and macrosegregation characteristics are analysed. Evolution of segregation patterns indicates the nature of composition distribution in the solidifying domain and provides quantitative estimation of the macrosegregation. Simulation case-studies points towards the fact that the non-equilibrium effects on account of solutal undercooling strengthen the advective effect, which in turn can lead to enhanced value of macrosegregation. The model predicted results are also compared with the available experimental data and good match can be observed.

ACKNOWLEDGEMENTS

The author would like to thank the management of Tata Steel, India, for giving permission to publish this work.

REFERENCES

- Bennon, W. D. and F. P. Incropera (1987). A continuum model for momentum, heat and species transport in binary solid-liquid phase-change systems-I. Model formulation. *International Journal of Heat Mass Transfer* 30, 2161-2170.
- Brenner, H. (1970) Rheology of two-phase systems. *Annu. Rev. Fluid Mech.* 2, 137-176
- Brent, A. D., V. R. Voller and K. J. Reid (1988). The enthalpy porosity technique for modelling convection-diffusion phase change: application to the melting of a pure metal. *Numerical Heat Transfer* 13, 297-318.
- Brody, H. D. and M. C. Flemings (1966) Solute

- redistribution in dendritic solidification, *Transaction Metall Soc AIME* 236, 615-624.
- Chakraborty, S. and P. Dutta (2002) The effect of solutal undercooling on double-diffusive convection and macrosegregation during binary alloy solidification: a numerical investigation. *International Journal of Numerical Methods Fluids* 38, 895-917.
- Choudhary, S. K. and D. Mazumdar (1994) Mathematical modelling of transport phenomena in continuous casting of steel. *ISIJ International* 34, 584-592.
- Clyne, T. W and W. Kurz (1981) Solute redistribution during solidification with rapid state diffusion *Metall. Trans. A* 12, 965-971.
- Ferreira, I. L., A Garcia and B. Nestler (2004). On macro segregation in ternary Al-Cu-Si alloys: Numerical and experimental analysis. *Scripta Mater.* 50, 407-411.
- Flemings, M. C. (1974). *Solidification Processing*. McGraw-Hill, New York, USA.
- Gadgil, A. and D. Gobin (1984). Analysis of two-dimensional melting in rectangular enclosures in presence of convection. *Journal of Heat Transfer* 106, 20-26.
- Ganaoui, M. EI., G. P. Bontoux, A. Lamazouade, E. Leonardi and, G. De Vahl Davis (2002). Computational model for solutal convection during directional solidification. *Numerical Heat Transfer B* 41, 325-338.
- Ganesan, S. and D. R. Poirier (1990). Conservation of mass and momentum for the flow of interdendritic liquid during solidification. *Metall. Trans. B.* 21, 173-181.
- Ganguly, S., A. Sengupta and S. K. Choudhary (2013) A generalized approach for macroscopic modelling of solidification of ternary alloys with dendritic arm coarsening. *ISIJ International* 53, 823-829.
- Kang, K. G., H. S. Ryou and N. K. Hur (2005). Coupled turbulent flow, heat and solute transport in continuous casting processes with an electromagnetic brake. *Numerical Heat Transfer A* 48, 461-481.
- Kobayashi, S. (1988). Solute redistribution during solidification with diffusion in the solid phase. *Journal of Crystal Growth* 88, 87-96
- Morvan, D., M. EI. Ganaoui and P. Bonboux (1999). Numerical simulation of a 2D crystal growth problem in vertical furnace: Latent heat effect and crystal melt interface morphology. *International Journal of Heat and Mass Transfer* 42, 573-579.
- Oldenburg, C. M., F. J. Spera (1992). Hybrid model for solidification and convection. *Numerical Heat Transfer, Part B* 21, 217-229.
- Patankar, S. V. (1980). *Numerical Heat Transfer and Fluid Flow*. Hemisphere, New York, USA.
- Prescott, P. J. and F. P. Incropera (1996). *Advances in Heat Transfer*. Academic Press, New York
- Rappaz, M. (1989). Modelling of microstructure formation in solidification process. *International Materials Review* 34, 93-123.
- Voller, V. R., A. D. Brent and C. Prakash (1989). The modelling of heat, mass and solute transport in solidification systems. *International Journal of Heat Mass Transfer* 32, 1719-1731.